International Journal of Computing and Digital Systems
ISSN (2210-142X)
Int. J. Com. Dig. Sys. 15, No.1 (Apr-24)

http://dx.doi.org/10.12785/ijcds/1501105

Semi-symmetrical Coprime Linear Array with Reduced Mutual Coupling Effect and High Degrees of Freedom

Fatimah Abdulnabi Salman[1] **and Bayan Mahdi Sabbar**[2]

[1]*System Engineering Department, College of Information Engineering, Al-Nahrain University, Baghdad, Iraq*
[2]*Medical Instrumentation Techniques Engineering Department, Al-Mustaqbal Universityy, Baghdad, Iraq*

Received 29 Nov.2022, Revised 9 Mar. 2024, Accepted 18 Mar. 2024, Published 1 Apr. 2024

Abstract: Direction finding based on coprime array has received great interest due to the higher degrees of freedom and larger aperture size as compared with the uniform linear array. In this paper, a new semi-symmetric coprime array (SSCA) configuration is proposed to reduce the mutual coupling impact for passive sensing by exploiting the relocation of the redundant elements. First, the difference co-array of the prototype coprime array (PCA) is examined and the redundant elements are identified. Based on this examination, the second subarray (N-subarray) is split into two subarrays on opposite axes, and the zero-lag location is changed to a new location (MN+N) to construct large contiguous lags in the difference co-array. The reduction of the mutual coupling effects is tested according to the weight function of the first three lags of the SSCA array which is equal to one since there are no more redundant elements pairing in the antenna array. The closed-form expression for the hole position, the contiguous lags and unique lags are formulated and analyzed. The investigation of the SSCA is performed. The analytical expressions of the contiguous lags, unique lags, and aperture size are derived. The numerical and simulation results demonstrate that the proposed SSCA array can attain less mutual coupling leakage as compared to other array types.

Keywords: DOA, Coprime array, Mutual coupling, Difference co-array

1. Introduction

Direction of arrival (DOA) estimation methods using antenna arrays have a wide range of applications in sonar, radar, wireless communication, navigation, radio direction finding and other research areas [1],[2],[3]. The most popular used array configuration is the uniform linear array (ULA) in which the distance between elements is half of the wavelength of signals. Therefore, the ULA array aperture size depends on the number of elements in the antenna array. However, there are several issues with the ULA configuration that affect the DOA estimation accuracy, first the distance between elements is restricted to half wavelength to prevent spatial aliasing. Secondly, the number of resolved signals is limited due to the number of physical elements. Thirdly, the separation between the elements is small which exposes the ULA array to the mutual coupling effect [4], [5].

Traditional DOA estimation methods such as MUSIC [6] and ESPIRT [7] have been used to resolve the signals with high resolution but with limitations to the number of detectable sources [8]. To undertake these issues, sparse arrays (non-uniform linear arrays NLAs) have been suggested to produce undetermined DOA estimation. Sparse arrays can produce a higher degree of freedom (DOFs) through the difference co-array (DCA) concept. Different lags are generated from pairwise differences in element positions that enhance the degrees of DOFs [9]. Sparse arrays such as minimum redundancy array (MRA) [10] and minimum hole array (MHA) [11] have been proposed to maximize the number of the contiguous lags and minimize the number of holes in the DCA respectively. However, these array designs lack the formal expression for the element locations and the amount of DOFs. Thus inappropriate array design would be presented when a great amount of elements are used in an antenna array [12] .

Over the last decade, nested arrays (NAs) [13],[14] and coprime arrays (CAs) [15] have drawn attention in the field of array signal processing due to their properties such as closed formal expression for element positions and virtual DCA, large central uniform segment, and mitigation of mutual coupling. The conventional NA [14] provides a hole-free array, but it faces a higher mutual coupling effect due to the dense sparse array with a distance of half wavelength. Subsequently, different array designs have

E-mail address: faty_salman@nahrainuniv.edu.iq, prof.dr.bayan.mahdi@uomus.edu.iq

come out based on the traditional NA array structure such as improved nested array (INA) [16] that adds one element to the antenna array to get more DOFs, super nested array (SNA) [17] which have the same lag generation as the NA with significant reduction of the element pair separation, augmented nested array (ANA) [18] that split the dense array and rearrange the position of the elements to reduce mutual coupling, and generalized nested array (GNA) [19] in which the spacing of the element can be no less than one-wavelength. The main issue in GNA is the elimination of uDOFs and the critical holes in its DCA. Nevertheless, in these array designs, the pairs of elements that have small distances generate considerable mutual coupling effects.

On the other side, coprime array is considered as another sparse array consisting of two interleaved ULA (M,N) with inter-elements spacing of Nd and Md respectively which has been widely investigated. Several modified array structures have been made to the conventional CA to improve the uniform segment and fill some holes in the DCA. Augmented coprime array (ACA) which extends the number of the elements in M-subarray has increased the number of contiguous lags but still has a considerable mutual coupling effect [20].

Two generalized coprime arrays with compressed inter-element spacing (CACIS) and displaced subarrays (CADiS) have been proposed in [21]. For CACIS configuration, the distance of the element in N-subarray is compressed by a compression factor that kept the minimum distance between the elements which results in elements overlapping in the self and cross lags differences. In CADiS configuration, the N-subarray is shifted by a predefined distance to enlarge the minimum distance between the subarrays to expand the aperture size and increase the number of unique lags [22]. However, it breaks the DCA into segments and critical holes exist that disturb the contiguous lags which degrades the performance of DOA estimation methods based on spatial smoothing [15],[23].

In [24] the authors proposed a thinned coprime array (TCA) exploiting the redundancy of the physical element pairs difference with small distance since these redundant elements do not contribute to the DCA. In [25] the authors proposed two array structures named k-times extended coprime array (kECA) and a complementary coprime array (CCA). In the two subarrays, extra elements are added to fill the holes. The main drawback of these array structures is the extra cost due to the additional physical elements. Also, the mutual coupling effect is due to the extra element pairs with a small distance in kECA and the close elements distribution with a distance of half wavelength in CCA structure.

In [26] the authors developed a hole-free coprime array (HFCA) based on a known number of elements. HFCA array achieved a high number of uDOFs by computing the optimal values of M and N. However, the mutual coupling effect did not be considered in the array design. In [27] the authors suggest an optimized array by modifying and adjusting the spacing between array elements of the sparse array to estimate DOA without spatial aliasing. In [28], the authors propose an array configuration using a branch and bound optimization algorithm. This array configuration is based on generalizing the minimum sensor array that provides the same number of resolved signals with a small number of elements.

In [29], the authors propose an improved symmetric flipped nested array (ISFNA) to increase the number of DOF. This array requires a set of ULAs that are influenced by the mutual coupling effect that degraded the estimation accuracy. The authors in [30] proposed an enhanced CACIS array by reordering the frequent element while keeping the element distance compressed. But still has a higher mutual coupling effect. In [31], the authors proposed several low redundancy arrays under particular configurations with a definite condition. The different classes are obtained when the second array is greater than 18.

As a result, the authors in [32] outlined some criteria to be considered in designing sparse arrays such as the closed form for elements positions, large contiguous lags, the hole issues, and the small weight function for the first three lags to mitigate the mutual coupling effect.

In order to construct a new coprime array configuration that has a uniform spacing and reduced mutual coupling effect as compared to other array types, a new array structure named semi-symmetric coprime array (SSCA) based on the conventional coprime array is proposed. In this paper, the prime contributions are listed as follows:

1) From the perspective of extending the virtual array structure, the range of contiguous lags is increased by dividing one of the two subarrays to be semi-symmetrical in axis. Then the closed-form expression for the hole-position, the contiguous lags and the unique lags are analyzed.
2) The relationship between the contiguous lags and the element position at the zeroth position is analyzed, and the proposed array is developed by relocating the zeroth position to a new location.
3) The number of contiguous lags, unique lags and weight function of the first three lags of the designed array are formulated and compared with array configurations.

The structure of the paper is arranged in several sections as in the following: Section 2 presents the data model of the prototype coprime array and the mutual coupling. In Section 3, the proposed semi-symmetric coprime array (SSCA) and its properties are presented. Section 4 demonstrates the performance analysis of the SSCA array in terms of mutual coupling leakage and spatial spectrum through simulation. Finally, the concluded remarks are presented in Section 5.

Notations: we use upper-case (lower-case) bold characters to denote matrices (vector). $[.]^T$, $[.]^*$ and $[.]^H$ stand for the transpose, conjugate and conjugate transpose respectively. diag(.) and vec(·) mean a diagonal matrix and the vectorization operator. E{·} represents the expectation operator. I_K indicates the identity matrix with size $K \times K$. $\odot$ and $\otimes$ represent the Khatri-Rao product and Kronecker product respectively. $\lfloor . \rfloor$ is the floor function. $\| . \|_F$ represents the

Figure 1. Prototype coprime array configuration

Frobenius norm.

2. Prototype Coprime Array Configuration

A prototype coprime array (PCA) [14] is composed of a pair of coprime integer M and N elements with elements distance Nd and Md respectively, where d is the minimum distance in the PCA and equals half the wavelength $d = \lambda/2$. The two subarrays shared the reference elements at the zeroth position; therefore, the entire amount of elements in the antenna array is $K = M + N - 1$ as shown in figure 1. The element's position is denoted as [33]:

$$P = \{Mnd \mid 0 \le n \le N-1\} \cup \{Nmd \mid 0 \le m \le M-1\} \quad (1)$$

A. Data Model

Assume that Q uncorrelated sources impinging on PCA from directions $\theta_1, \theta_2, \ldots, \theta_Q$, then the observed data vector is given by [20]:

$$\mathbf{X}(t) = \sum_{q=1}^{Q} \mathbf{a}(\theta_q) s_q(t) + \mathbf{n}(t) = \mathbf{A}\mathbf{s}(t) + \mathbf{n}(t) \quad (2)$$

where

$$\mathbf{a}(\theta) = [1, e^{j2\pi p_2 \sin(\theta_q)/\lambda, \ldots, j2\pi p_{M+N-1} \sin(\theta_q)/\lambda}] \quad (3)$$

$\mathbf{a}(\theta_q)$ is the directional vector, $\mathbf{A} = [\mathbf{a}(\theta_1), \ldots, \mathbf{a}(\theta_Q)]$ is the directional matrix, and $\mathbf{p} = [p_1, \ldots, p_K]^T$ denote the positions of the elements in PCA, where $p_i \in p$, $i = 1, \ldots, K$. s(t)is the source vector where $\mathbf{s}(t) = [s_1(t), \ldots, s_Q(t)]^T$. $\mathbf{n}$(t) is the noise vector which is additive white Gaussian noise. The correlation matrix ***(R)*** of the observed vector is determined as:

$$\mathbf{R} = E\{\mathbf{X}(t)\mathbf{X}^H(t)\} = \mathbf{A}\mathbf{R}_s\mathbf{A}^H + \sigma_n^2\mathbf{I}_K \quad (4)$$

$$= \sum_{q=1}^{Q} \sigma_q^2 \mathbf{a}(\theta_q)\mathbf{a}^H(\theta_q) + \sigma_n^2\mathbf{I}_K \quad (5)$$

where $\mathbf{R}_s = E\{\mathbf{s}(t)\mathbf{s}^H(t)\} = diag(\sigma_1^2, \ldots, \sigma_Q^2)$ is the source correlation matrix, and σ_q^2 represnts the power of the qth source ($q = 1, \ldots, Q$). $\sigma^2\mathbf{I}_K$ is the noise correlation matrix, $\mathbf{I}_K$ is identity matrix with size $K \times K$. The estimated correlation matrix for T snapshots is expressed as [23]:

$$\widehat{\mathbf{R}} = \frac{1}{T}\sum_{t=1}^{T} \mathbf{X}(t)\mathbf{X}^H(t) \quad (6)$$

Vectorizing $\widehat{\mathbf{R}}$ yields

$$v = vec(\widehat{\mathbf{R}}) = \mathbf{B}\mathbf{p} + \sigma_n^2\widehat{\mathbf{I}}_K \quad (7)$$

where$\mathbf{B} = \mathbf{A} \odot \mathbf{A}^H = [\mathbf{a}(\theta_1) \otimes \mathbf{a}^*(\theta_1), \ldots, \mathbf{a}(\theta_q) \otimes \mathbf{a}^*(\theta_q)]$ is the directional matrix of the virtual array with a large aperture size, $\mathbf{p} = [\sigma_1^2, \ldots, \sigma_Q^2]^T$ and $\sigma_n^2(I_K)$ is the noise matrix. z is considered as the observed data for a coherent source of single snapshots with deficient matrix rank and the spatial smoothing is utilized to retrieve the full rank. Anyway, the spatial smoothing can be performed only on the contiguous lags. Assuming $U = [-L_u, L_u]$ is the range of the contiguous lags in the DCA, then a new vector z_U with $(2L_U + 1) \times 1$ can be formed as follows [23]:

$$\mathbf{z}_U = \mathbf{B}\mathbf{p} + \sigma^2\mathbf{I}_K \quad (8)$$

where $\mathbf{B}$ is the virtual directional matrix with respect to the contiguous lags with size $(2L_U + 1) \times Q$ and $\mathbf{I}_K$ is a vector with $(2L_U + 1) \times 1$. For contiguous lags for one side can be expressed as z_{Uv}, $v = 1, 2, \ldots, L_U + 1$, then the spatial smoothing matrix can be illustrated as:

$$\mathbf{R}_z = \frac{1}{(L_U + 1)}\sum_{v=1}^{L_U+1} z_{Uv}z_{Uv}^H \quad (9)$$

where $\mathbf{R}_z$ is utilized to estimate the DOAs of the sources by performing MUSIC algorithm. It is important to notice that the ULA segment in the DCA has a great impact on the estimation process [23].

B. Mutual Coupling

In the antenna array, the element output is affected by its neighboring elements. When the elements are nearby to each other's, the mutual coupling can degrade the performance of antenna radiation patterns performance. The array output observation in eq.(2) can be modeled to incorporate the mutual coupling impact as follows.

$$\mathbf{X}(t) = \mathbf{C}\mathbf{A}\mathbf{s}(t) + \mathbf{n}(t) \quad (10)$$

where $\mathbf{C}$ is $K \times K$ mutual coupling matrix. It can be modeled regarding the distance between the elements in an antenna array. For ULA structure, $\mathbf{C}$ is a B-bounded symmetrical Toeplitz matrix for ULA structure defined as:

$$\mathbf{C} = \begin{cases} c_{|d_i - d_j|}, & |\, d_i - d_j \,| \le B \\ 0, & \text{otherwise} \end{cases} \quad (11)$$

where $p_i, p_j \in P$ and $c_l = c_1 e^{(-j(l-1)\pi/8)}/l$ for $l \in (2, B)$, c_1 represents the governing mutual coupling point under the single unit of elements distance status. $c_0, c_1, \ldots c_B$ coupling coefficients fulfill $c_0 = 1 > |\, c_1 \,| \ldots | \, c_B \,|$ and their magnitude is related to their elements partitions, i.e., $|\, ck/cl \,| = l/k$ for $k, l > 0$ [17].

C. Weight function

The weight function is an important feature in sparse array configurations and is directly related to the array mutual coupling [17] and antenna economy [13]. The weight function w(m) of an antenna array is the amount of elements

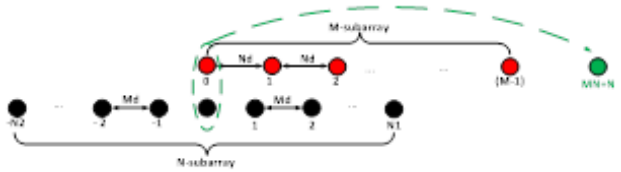

Figure 2. proposed semi-symmetric coprime array

pair in P with m separation [20].

$$w(m) = \{(d_i - d_j) \in P^2 : d_i - d_j = m\}, m \in D \tag{12}$$

where $P^2 = P \times P$ for any set P. For any $m \in D$, $w(m) > 0$, otherwise it is zero. The first three lags weight function specifically w(1),w(2) and w(3) have a significant impact on the array performance, and w(1) affords an immense impact [21].

3. Proposed Semi-Symmetrical Coprime Array Configuration

A new semi-symmetrical coprime array (SSCA) configuration is proposed. This configuration is formed on a symmetrical N-subarray while the M-subarray is left unchanged. Then the 0-lag position element of the aforementioned array is relocated to a new location to $MN+N$. The proposed array has many outstanding properties. The elements' positions, the consecutive lags, weight function and aperture size can be formally expressed.

A. Proposed array Configuration

The proposed array consists of $K = N + M - 1$ elements, where $N \geq M \geq 3$. Figure 2 shows the proposed SSCA configuration where N-Subarray has been divided into 2-subarrays being symmetrical in x-axis with Md inter-element spacing and the 0-element position has been changed to the position $MN+N$. The position set (P^{SSCA}) of the SSCA array is expressed in the following relationship:

$$\mathbf{P}^{SSCA} = \{P_1^{SSCA} \cup P_2^{SSCA} \cup P_3^{SSCA} \cup P_4^{SSCA}\} \tag{13}$$

where

$P_1^{SSCA} = \{mNd, 1 \leq m \leq M-1)\}$
$P_2^{SSCA} = \{n_1 Md, 1 \leq n_1 \leq N_1)\}, N_1 = \lfloor N/2 \rfloor$
$P_3^{SSCA} = \{-n_2 Md, 1 \leq n_2 \leq N_2)\}, N_2 = N - N_1 - 1$
$P_4^{SSCA} = \{MN_2 + N + M + \lfloor N/2 \rfloor M\}d$

The zero reference of the two subarrays is changed to the end of the two subarrays to fill some holes and increase the range of the contiguous lags range and extend the aperture array size as provided in the next section. An example of the SSCA array configuration with $M = 3, N = 4$, is shown in figure 3. $N_1 = \lfloor N/2 \rfloor = 2$, and $N_2 = N - N_1 - 1 = 1$. According to eq.(13), the elements are set as follows, $P^{SSCA} = \{-3, 3, 4, 6, 8, 16\}d$, where $P_1^{SSCA} = \{4, 8\}d$, $P_2^{SSCA} = \{3, 6\}d$, $P_3^{SSCA} = \{-3\}d$, and $P_4^{SSCA} = 16d$. The top figure shows the physical elements position, the middle figure shows the corresponding DCA and the bottom figure shows the weights function.

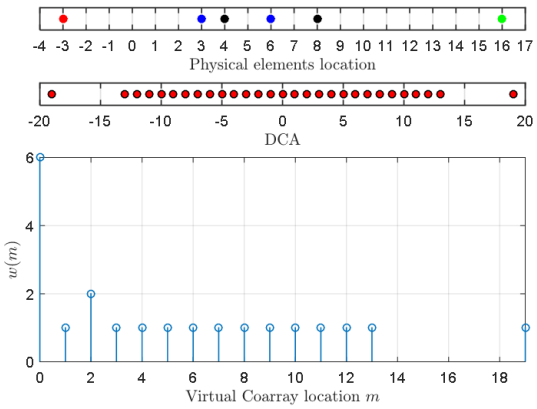

Figure 3. The elements position, DCA and the weight function of a SSCA array with $K = 6, M = 3$, and $N = 4$

B. SSCA array properties

In this subsection, the SSCA properties are explained to show its merits against other array configurations.

1) Degrees of freedom (DOFs) is the amount of unique lags in D. For SSCA array, it depends on the value of N-subarray whether it's odd or even integer. If N is odd, the unique lags closed-form denoted by $2MN + 4\lfloor N/2 \rfloor + 1$, on the other hand, when N is even, the unique lags $2MN + 2\lfloor N/2 \rfloor + N - M$ for $M \geq 3$.
2) Uniform DOF (uDOFs) is the central ULA segment (contiguous lags) in D. The SSCA array can provide a contiguous lags within the range $[-(N_2M + 2N + M + 1) : N_2M + 2N + M + 1]$. The uDOF in the D is denoted by U, where
$$U = 2N_2M + 4N + 2M - 1 \tag{14}$$
3) Aperture size is the length of the coprime array related to the last element location. The SSCA array can provide a high aperture size equal to $MN + 2N - \lfloor N/2 \rfloor - 1$.
4) Another advantage of the proposed SSCA array is the less affect to mutual coupling due to the reduction of the weight function as compared to other array types. For SSCA array with $M \geq 3$, the weight functions w(m) for m=1,2 and 3 is as follows:

$$\begin{cases} w(1) = 1, & M \geq 3 \text{and} N \geq M+1 \\ w(2) = \begin{cases} = 2 & M = 3 \text{and} N = M+1 \\ = 1, & \text{otherwise} \end{cases} \\ w(3) = \begin{cases} = N-3 & M = 3 \text{and} N \geq 5 \\ = 1, & \text{otherwise} \end{cases} \end{cases} \tag{15}$$

Table I shows a comparison of the lags generation

TABLE I. LAG GENERATION OF FORMAL-EXPRESSION COMPARISON OF DIFFERENT ARRAY TYPES

Array type	No. of elements	No. of uDOF	No. of DOF(Unique lags)	Aperture size
PCA[15]	$M+N-1$	$2(M+N)-1$	$MN+M+N-2$	$MN-M$
NA[14]	$N1+N2$	$2N2(N1+1)-1$	$2N2(N1+1)-1$	$N2(N1+1)$
ACA [20]	$2M+N-1$	$2(MN+M)-1$	$3MN+M-N$	$2MN-N$
INA[16]	$N1+N2+1$	$22N2(N1+1)-1$	$2N2(N1+1)-1$	$N1N2+N2+N1-1$
SNA[17]	$N1+N2$	$2N2(N1+1)-1$	$2N2(N1+1)-1$	$N2(N1+1)$
GNA[19]	$N1+N2$	-	$2N2(N1+1)-1$	$\alpha N1+\beta(N2-1)+1$
CACIS[21]	$M+N-1$	$2MN-2M/p(N-1)-1$	$2MN-M/p(N-1)-N$	$MN-M$
CADiS[21]	$M+N-1$	$MN-(M/p-1)(N-2)+1$	$2MN+2M-5$	$(N-1)M/p+(M-2)N+M+N$
kECA[25]	$kM+N-1$	$2(k-1)MN+2M-1$	$(2k-1)MN+M-N$	$kMN-N$
CCA [25]	$(k+1)M+N-2$	$2kMN-2N+1$	$2kMN-2N+1$	$kMN-N$
TCA[24]	$M+N+\lfloor M/2\rfloor 1$	$2MN+2M-1$	$3MN+M-N$	$2MN-N$
HFCA[26]	-	$2N(T+1-N-\lfloor M/2\rfloor)+6M-1$	$2N(T+1-N-\lfloor N/2\rfloor)+6M-1$	$3M+N(T+1-N-\lfloor N/2\rfloor)-1$
SSCA	$M+N-1$	$2N_2M+4N+2M-1$	N-odd $2MN+4\lfloor N/2\rfloor+1$ N-even $2MN+4\lfloor N/2\rfloor+1+N-M$	$MN+2N-\lfloor N/2\rfloor-1$

formal expressions in terms of the total number of the elements, uDOF, DOFs (unique lags) and aperture size of the proposed SSCA structure with other array types.

C. Difference Co-array Analysis

In this subsection, SSCA array structure is analyzed before and after N-subarray splitting, afterward, the resultant virtual array will be analyzed before and after removing the reference elements at 0-position regarding the amount of contiguous lags and holes position to illustrate the structure design and performance marks of SSCA array. The mathematical expression for the DCA, the number of uDOFs, unique lags and aperture size are derived to improve the array design.

1) Analyzing DCA before N-subarray splitting

For the PCA consists of (M,N) pair of elements, the elements are located at:

$$S_{PCA} = S_1 \cup S_2 \tag{16}$$

where $S_1 = \{mNd, 0 \le m \le M-1)\}$, $S_2 = nMd, 0 \le n \le N-1)$. The DCA of the PCA can be constructed from the self-difference sets D_s which can be defined as $D_s = s_i - s_j \mid (i,j) \in S$ and the cross-difference sets D_c as follows:

$$\begin{aligned} D_{PCA} &= D_s \cup D_c = D_{11} \cup D_{22} \cup D_{12} \cup D_{21} \\ &= (S_1 - S_1) \cup (S_2 - S_2) \cup (S_1 - S_2) \cup (S_2 - S_1) \end{aligned} \tag{17}$$

where
$D_{11} = S_1 - S_1 = \{mNd, 0 \le m \le M-1\}$
$D_{22} = S_2 - S_2 = \{nMd, 0 \le n \le N-1\}$
$D_{12} = S_1 - S_2 = \{mNd - nMd, 0 \le m \le M-1, 0 \le n \le N-1\}$
$D_{21} = S_2 - S_1 = \{nMd - mNd, 0 \le n \le N-1, 0 \le m \le M-1\}$
It can be noticed that the lag sets D_{12} and D_{21} include both the cross-lags and self-lags and D is symmetrical about x-axis, so only one side will be analyzed. Since the self-difference lags are exists in the cross and self-difference lags, then D_{12} can be rewritten, after excluding the lags that appear in the self-difference, as shown in the following set:

$$\overline{D}_{12} = \{mNd - nMd, 1 \le m \le M-1, 1 \le n \le \lfloor N/2 \rfloor\} \tag{18}$$

The set $\overline{D}_{12}$, would not affect the difference lags set for PCA array. Then, if $N - \lfloor N/2 \rfloor - 1$ elements are removed from N-subarray the contiguous lags would not change, besides removing these elements will reduce the weight function of the cross-difference lags due to the reduction of the overlapped elements in the sets D_{11} and D_{22}. Thus the DCA after removing these elements will be denoted as:

$$\overline{D} = D_{11} \cup \overline{D}_{22} \cup \overline{D}_{12} \tag{19}$$

where $\overline{D}_{22} = \{n_1 Md - n_1 Md, 0 \le n_1 \le \lfloor N/2 \rfloor\}$. Only the self-difference D_{22} set will be affected by removing $N - \lfloor N/2 \rfloor - 1$ elements and additional holes will exist in the DCA which is located at the end of the N-subarray. The resulting array has holes in the sets H_1^R, H_2^R, and H_3^R.

$$H_1^R = \{h_1 \mid h_1 = \pm(aM + bN), a \in \langle 1, \lfloor N/2 \rfloor \rangle, b \in \langle 1, M-2 \rangle\} \tag{20}$$

$$H_2^R = \{h_2 \mid h_2 = \pm(cM), c \in \langle \lfloor N/2 \rfloor + 1, N-1 \rangle\} \tag{21}$$

$$H_3^R = \{h_3 \mid h_3 = M + N + \lfloor N/2 \rfloor M\} \tag{22}$$

From eq.(21), it can be concluded that the holes are the removed elements that was reside at the end of N-subarray. Let $c = c_0 = \lfloor N/2 \rfloor + 1$ and $c = N - c_0$, then eq.(21) can be rewritten as $-(N\lfloor N/2 \rfloor - 1)M$, and $-(N - \lfloor N/2 \rfloor - 1)M \in P_3$ which refers to as the element position in the N-subarray at the negative side. Thus, the holes in H_1^R and H_2^R can be filled for $-\langle N - \lfloor N/2 \rfloor - 1, 1 \rangle M$ elements and an augmented contiguous virtual array ranging $-(\lfloor N/2 \rfloor M + M + N - 1)$ to $\lfloor N/2 \rfloor M + M + N - 1$ can be obtained.
Figure 4 illustrates an example of SSCA array configuration (physical elements location, DCA and weight function) before and after splitting N-subarray and after relocating the 0-lag position when M=6, and N=7. Figure 4(a) presents the PCA configuration, where the elements are located at $S_1 = \{0, 6, 12, 18, 24, 30, 36\}d$, $S_2 = \{0, 7, 14, 21, 28, 35\}d$, the contiguous lags ranging from $-(M+N-1)$ to $(M+N-1)$ and the holes set is $H^{PCA} = \pm(aM + bN), a \in (1, N - \lfloor N/2 \rfloor), b \in$

$(1, M-2)\}$ and H^{PCA} within range ⟨M,MN-N⟩. The weight function for the first three lags is w(1)=w(2)=w(3)=2.

Figure 4(b) presents the array configuration when $N - \lfloor N/2 \rfloor - 1$ elements are removed from N-subarray, the location of the elements in N-subarray at $S_1 = [0, 6, 12, 18]d$, while the location of the elements in M-subarray is left unchanged, the contiguous lags is the same as the PCA and the holes are at $[13, 19, 20, 24, 25, 26, 27, 30, 31, 32, 33, 34, 36]d$ as defined in eqs.(20) to (22), where the three additional holes $[24, 30, 36]d$ exist in the DCA. The weight function for the three first lags is reduced to $w(1) = w(2) = w(3) = 1$. Figure 4 (c) presents the array configuration after splitting N-subarray to be located on the negative and positive side, the elements are located at $S_1 = \{-18, -12, -6, 0, 6, 12, 18\}d$, the contiguous lags is expanded from $[-12 : 0 : 12]$ to $[-30 : 0 : 30]$ and reduced the weight function for the three first lags. Figure 4 (d) presents the array configuration when removing the 0-lag, it can be seen that the contiguous lags do not change and only one hole exists at 35. While Figure 4 (e) shows the SSCA array configuration when relocating the 0-lag to $MN + N$ position, it can be shown that the range of the contiguous lags is extended to $[-37 : 0 : 37]$.

2) Analyzing DCA after splitting and Before removing 0-lag

The elements position before removing 0-lags is illustrated as follows:

$$S = S_1 \cup S_2 \cup S_3 \tag{23}$$

Where
$S_1 = \{mNd, 0 \le m \le (M-1)\}$,
$S_2 = \{n_1 Md, 0 \le n_1 \le N_1\}, N_1 = \lfloor N/2 \rfloor$
$S_3 = \{-n_2 Md, 0 \le n_2 \le N_2\}, N_2 = N - N_1 - 1$
The DCA (D) is composed of the self-difference sets D_s and the cross-difference sets D_c as follows:

$$D = D_s \cup D_c = D_{11} \cup D_{22} \cup D_{33} \cup D_{21} \cup D_{31} \cup D_{32} \tag{24}$$

where
$D_{21} = S_2 - S_1 = \{n_1 Md - mNd, 0 \le n_1 \le \lfloor N/2 \rfloor, 0 \le m \le M-1\}$
$D_{31} = S_3 - S_1 = \{-n_2 Md - mNd, 0 \le n_2 \le N - \lfloor N/2 \rfloor - 1, 0 \le m \le M-1\}$
$D_{32} = S_3 - S_2 = \{-n_2 Md - n_1 Md, 0 \le n_1 \le N - \lfloor N/2 \rfloor - 1, 0 \le n_1 \le \lfloor N/2 \rfloor\}$
$D_{11} = S_1 - S_1 = \{mNd, 0 \le m \le M-1\}$
$D_{22} = S_2 - S_2 = \{n_1 Md, 0 \le n_1 \le \lfloor N/2 \rfloor\}$
$D_{33} = S_3 - S_3 = \{-n_2 Md, 0 \le n_2 \le N - \lfloor N/2 \rfloor - 1\}$
Since DCA is a symmetric, only one side is provided. From the above sets, it can be observed that the 0-lag exists in the D_s and D_c, and the following relations is obtained, $D_{33} \subseteq D_{22}, D_2 2 \subseteq D_{32}$, and $D_{11} \subseteq D_{31}$, thus the following can be defined as: $D_1 = \{n_1 Md - mNd, 0 \le n_1 \le \lfloor N/2 \rfloor - 1, 0 \le M-1\}$
$D_2 = \{-n_2 Md - mNd, 0 \le n_2 leq N_2 - 1, 0 \le m \le M-1\}$

$$D_3 = \{Mnd, 0 < n < N-1\} \tag{25}$$

Actually, the self-difference lag set includes a large number of duplicated lags, besides it exists in the cross-difference lag set [12], [13], [14]. To eliminate this duplication, the following preposition is presented to explore the relationship of these sets in the DCA.

Preposition1: For $D_{33} \subseteq D_{22}, D_{22} \subseteq D_{32}, D_{32} = D_3$ When $N \ge 4$, we get the relation $N > \lfloor N/2 \rfloor > N - \lfloor N/2 \rfloor 1$. From the expressions $D_{33} \subseteq D_{22}, D_{22} \subseteq D_{32}$, One can get $D_{32} = D_3$.

Preposition2: For $D_{11} \subseteq D_{31}$, Before removing 0-lag, The number of uDOFs is $U = 2(N_2 M + N + M) - 1$ and the number of the unique lags when N is odd is $2MN - 1$ and when N-is even is $2MN - M$.

3) Analyzing DCA After removing 0-lag

After removing 0-lag, the elements position is denoted as $\overline{S}$, which is illustrated as follows:

$$\overline{S} = \overline{S}_1 \cup \overline{S}_2 \cup \overline{S}_3 \tag{26}$$

where
$\overline{S}_1 = \{mNd, 1 \le m \le M-1\}$
$\overline{S}_2 = \{n_1 Md, 1 \le n_1 \le N_1\}, N_1 = \lfloor N/2 \rfloor$
$\overline{S}_3 = \{-n_2 Md, 1 \le n_2 \le N_2\}, N_2 = N - N_1 - 1$
The DCA ($\overline{D}$) is expressed as:

$$\overline{D} = \overline{D}_s \cup \overline{D}_{=} \overline{D}_{11} \cup \overline{D}_{22} \cup \overline{D}_3 3 \cup \overline{D}_{21} \cup \overline{D}_{31} \cup \overline{D}_{32} \tag{27}$$

Where
$\overline{D}_{21} = \overline{D}_1 = \overline{S}_2 - \overline{S}_1 = \{n_1 Md - mNd, 1 \le n_1 \le \lfloor N/2 \rfloor, 1 \le m \le M-1\}$
$\overline{D}_{31} = \overline{D}_2 = \overline{S}_3 - \overline{S}_1 = \{-n_2 Md - mNd, 1 \le n_2 \le N - N_2 - 1, 1 \le m \le M-1\}$
$\overline{D}_{32} = \overline{S}_3 - \overline{S}_2 = \{-n_2 Md - n_1 Md, 1 \le n_1 \le N - N_2 - 1, 1 \le n_1 \le \lfloor N/2 \rfloor\}$
$\overline{D}_{11} = \overline{D}_3 = \overline{S}_1 - \overline{S}_3 = \{mNd, 0 \le m \le M-2\}$
$\overline{D}_{22} = \overline{S}_2 - \overline{S}_2 = \{n_1 Md, 1 \le n_1 \le \lfloor N/2 \rfloor\}$
$\overline{D}_{33} = \overline{S}_3 - S\overline{S}_3 = \{-n_2 Md, 1 \le n_2 \le N - N_2 - 1\}$
Similar relations to the previous preposition is obtained, where $\overline{D}_{33} \in \overline{D}_{22}, \overline{D}_{22} \cup \overline{D}_{32} = D_3$, and $\overline{D}_{22} \cup \overline{D}_{11} \cup \overline{D}_{31} = D_2$, so $\overline{D}$ can be defined as:

$$\overline{D} = \overline{D}_1 \cup \overline{D}_2 \cup \overline{D}_3 \cup \overline{D}_4 \tag{28}$$

When the 0-lag is removed, only one element is removed from the DCA at the position $N(M-1)$, which does not affect the contiguous lags of (D) for $M > 4$. If the 0-lag moved to the new position $(MN_2 + N + M + \lfloor N/2 \rfloor M)$, the range of the contiguous lags and unique lags will be increased by N and $N + M + 1$ respectively, besides the lag redundancy will be eliminated. The following sets expressed the DCA after moving the0-lag to the new position $\overline{D}_{41} = \overline{S}_4 - \overline{S}_1 = \{MNd + Nd - mNd, 1 \le m \le M-3\}$
$\overline{D}_{42} = \overline{S}_4 - \overline{S}_2 = \{MNd + Nd - n_1 Md, 1 \le n_1 \le \lfloor N/2 \rfloor\}$

$$\overline{D}_{43} = \overline{S}_4 - \overline{S}_3 = \{MNd + Nd - (n_2 Md), 1 \le n_2 \le N - \lfloor N/2 \rfloor - 1\} \tag{29}$$

The removed element at position $N(M-1)d$ are filled according to eq.(23) besides other holes are filled to extend

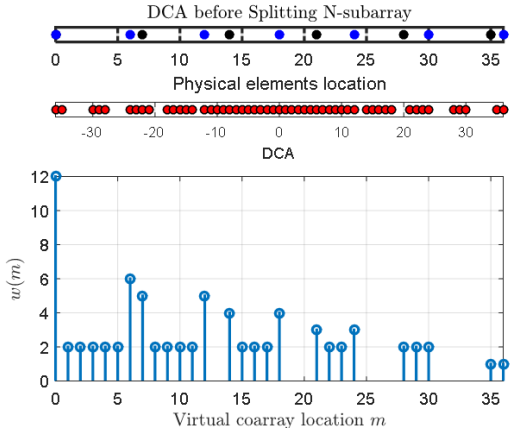

(a) Physical elements, DCA and weight function before splitting N-subarray

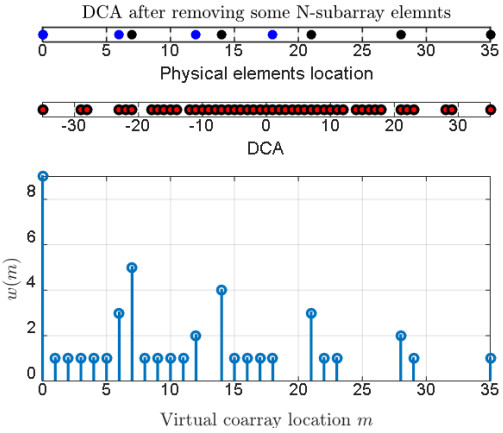

(b) Physical elements, DCA and weight function before splitting N-subarray

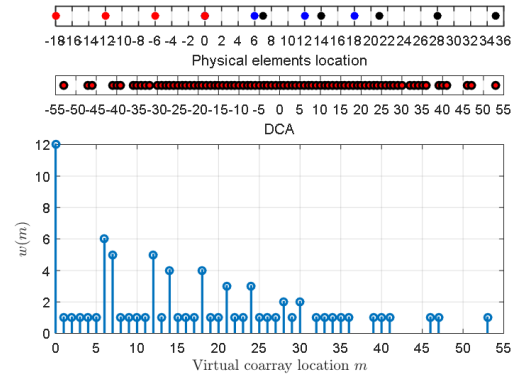

(c) Physical elements, DCA and weight function after splitting N-subarray

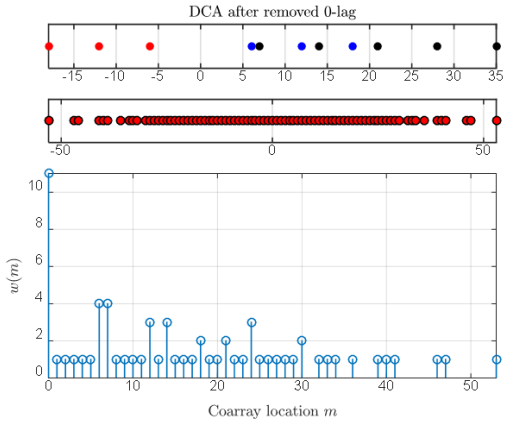

(d) Physical elements, DCA and weight function after removing 0-lag

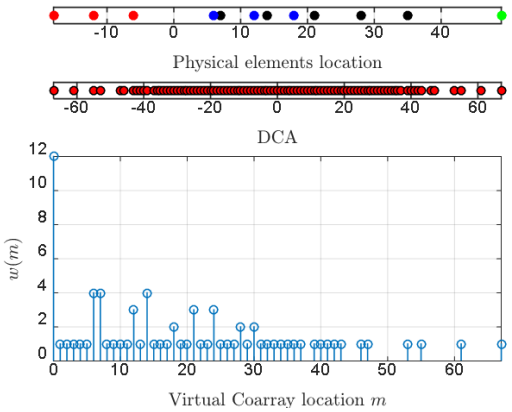

(e) Physical elements, DCA and weight function of the SSCA array

Figure 4. The SSCA DCA analysis steps

the contiguous lags range $[-(N_2M+2N+M+1)\colon 0\colon N_2M+2N+M+1]$ and the number of unique lags.

4) Analyzing weight function of SSCA array

The weight function $w(m)$ with small values is preferable since it has a direct impact on mutual coupling. In this subsection, the weight function of SSCA which is given in eq.(16) is analyzed. It is obvious that the distance between the fourth subarray and the other subarrays in SSCA is more than 8d since the last elements in these subarrays are located at $(M-1)Nd$, thus it will not affect the weight function of the first three lags. For M=3 and $N = M+1 = 4$, there is an interaction between two elements in the first subarray with an element in the second subarrays with spacing 2d that results in $w(2) = 2$. When M=3 and $N \geq 5$, the elements in the second subarray and the third subarray have spacing with 3d, when performing the self-difference, there is $N-3$ frequency occurrence of w(3). For the second subarray self-difference, there is $\lfloor N/2 \rfloor - 1$ occurrence of w(3) plus $(N-N_1-1)-1$ for the third subarray, and the total number of $w(3) = N-3$.

4. Numerical and Simulation Analysis

In this section, different array types are compared with the proposed SSCA array structure with respect to the lags being generated, DOF capacity, weight function, mutual coupling leakage, DOA estimation performance with the existence of mutual coupling and the root mean square error (RMSE).

A. Lags generation comparison

The lags generation comparison of the proposed SSCA structure with other array types such as PCA, ACA, CACIS, CADiS, TCA , CCA, k-times ECA and nested array is shown in figure 5 in terms of uDOFs, DOFs and aperture size. It is illustrated that the proposed SSCA array has significantly improved the number of uDOFs, DOF and aperture size as compared to other array designs where SS- algorithms can only perform on the contiguous lags. Another comparison regarding the DOF capacity of the different array structures is shown in Figure 6. DOF Capacity is a measure for comparing the sparsity of array structure. DOF capacity is defined as:

$$\gamma(P) = \frac{P^2}{DOFs} \tag{30}$$

where P is the total number of physical elements in the sparse array and DOFs denote the number of DOFs measured by the contiguous lags or unique lags. A small value of $\gamma(P)$, means a higher DOF capacity[24].The smaller the value of $\gamma(P)$, the higher DOF capacity for a particular number of elements in the antenna array. It can be shown in figure (6)a which represents the DOF capacity regarding the uDOF segment, that is super nested array has the lowest $\gamma(P)$, and higher capacity because it can achieve higher DOF at the cost of higher mutual coupling due to the dense sparse array, that increase the weight function of the first three lags in the virtual array. In figure (6) b which represents the DOF capacity regarding the unique lags (total DOFs), it can be shown that the proposed SSCA has the highest capacity since it can generate a large number of unique lags as compared to other array types.

B. Mutual coupling and weight function

The weight function is related to mutual coupling leakage which is used to evaluate the impact of mutual coupling. The following coupling coefficients are used to model the mutual coupling in eq.(11) $c_1 = 0.3e^{j\pi/3}$, $B = 100$, and $c_l = c_1 e^{-j(l-1)\pi/8)/l}$ for $2 \leq l \leq B$, where the range of the parameter c is between $[0.1\colon 1]$. When C is diagonal, the elements do not interpose with one another, so it does not introduce mutual coupling. Therefore, the off-diagonal elements energy identified the amount of the mutual coupling leakage as described by:

$$L = \frac{\| C - diag(C) \|_F}{\| C \|_F} \tag{31}$$

where $\| \, . \, \|_F$ and $diag(C)$ indicate the Frobenius norm of the C matrix and C is a diagonal matrix with zero off-diagonal components, respectively. Note that $0 \leq L \leq 1$, which means a small L indicates less mutual coupling impact. Table II shows the weight function of the first three lags and the mutual coupling leakage for different array types such as PCA, ACA, CADiS, NA, INA, SNA, TCA, HFCA and the proposed SSCA array. It can be noticed that when the number of the element is 10, the SSCA array has the lowest mutual coupling leakage value as defined in eq.(12). While the nested array has the highest value due to the dense array, it experiences severe mutual coupling impact. When the number of the elements is 12 and 16, CADis has the lowest mutual coupling since the weight function of the first two lags is zero which means no lags exist in the first and second position which breaks the contiguous segment. Apart from CADiS configuration, the proposed SSCA array has lower mutual coupling leakages as compared to other array types.

C. Spatial spectrum in the presence of mutual coupling

In this subsection, the MUSIC spectrums for different arrays structures are shown in figure 7. The amount of physical elements is set to 12 elements, the array structures are set as follows, PCA and proposed array (SSCA) are formed with M=6, N=7, ACA is formed with $M = 4, N = 5$, NA and SNA with $N1 = N2 = 6$, INA with N1=5; N2=6 and HFCA is formed with M=3; N=5. There are 21 sources signals that are uniformly distributed within the range $\bar{\theta} = [-0.3, 0.3]$ SNR is 10dB. A $c_{=}0.3e^{j\pi/3}$, and the number of snapshots is set to 1000. The spatial smoothing for the co-array MUSIC algorithm in [22] is performed to evaluate the spatial spectrum.

The first row shows the physical elements' position. The second row shows the weight functions of different sparse arrays. It is obvious that the proposed SSCA array present a great set of weight functions where the first three lags

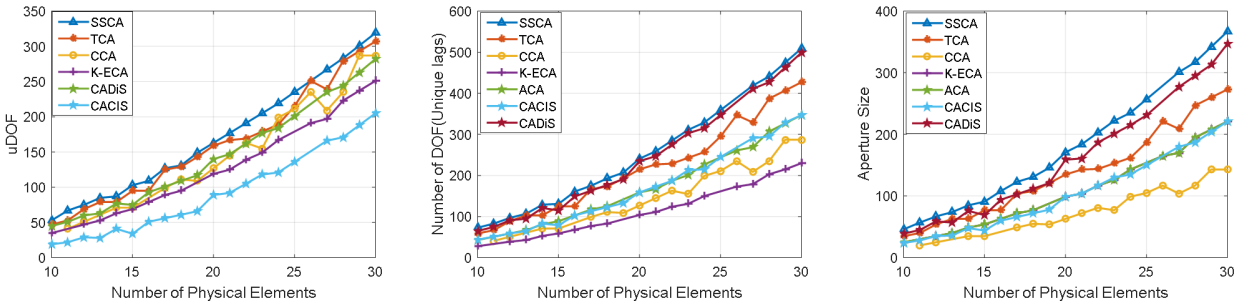

(a) uDOF vs number of physical elements (b) DOF vs number of physical elements (c) Aperture size vs number of physical elements

Figure 5. Comparison for lags generation vs. number of elements for different array types

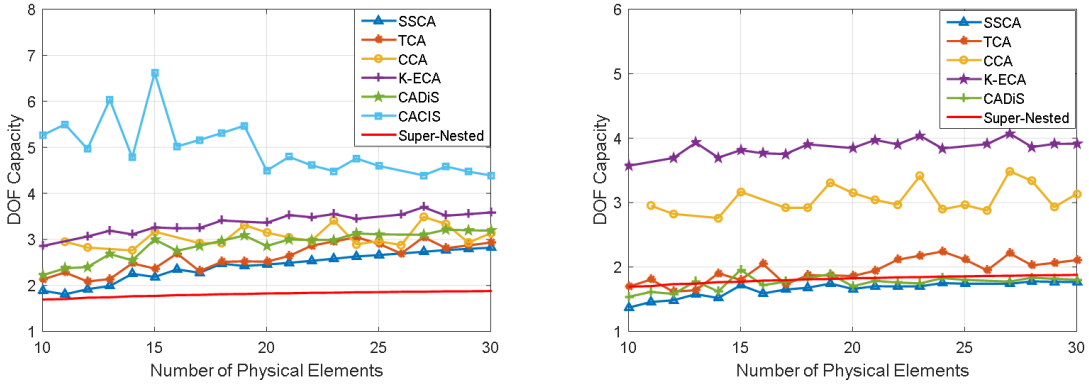

(a) DOF Capacity regarding contiguous lags (b) DOF Capacity regarding unique lags

Figure 6. Comparison for lags generation vs. number of elements for different array types

TABLE II. The first three lags weight Function and Mutual Coupling Leakage for different array types

Array type	PCA	CADiS	SSCA	HFCA	ACA	TCA	NA	SNA	UNA
10 elements		M=5, N=6		M=3, N=4	M=3,N=5	M=4,N=5	N1=N2=5		N1=4,N2=5
w(1)	2	0	1	3	2	1	5	1	4
w(2)	2	6	1	2	2	2	4	4	3
w(3)	2	0	2	4	5	1	3	1	2
L	0.23919	0.19119	0.18216	0.26857	0.24958	0.19729	0.32906	0.21283	0.29579
12 elements		M=6, N=11		M=3, N=8	M=4,N=9	M=4,N=11	N1=N2=8		N1=7,N2=8
w(1)	2	0	1	3	2	1	8	2	7
w(2)	2	0	1	2	2	2	7	6	6
w(3)	2	10	1	7	2	1	6	1	5
L	0.19627	0.13923	0.14905	0.22743	0.20487	0.17287	0.33493	0.21774	0.31391
16 elements		M=6, N=7		M=3, N=5	M=4,N=5	M=5,N=6	N1=N2=6		N1=5,N2=6
w(1)	2	0	1	3	2	1	6	2	5
w(2)	2	0	1	2	2	1	5	3	4
w(3)	2	6	1	4	2	1	4	3	3
L	0.22054	0.12611	0.16261	0.24883	0.22818	0.16867	0.33134	0.22839	0.30344

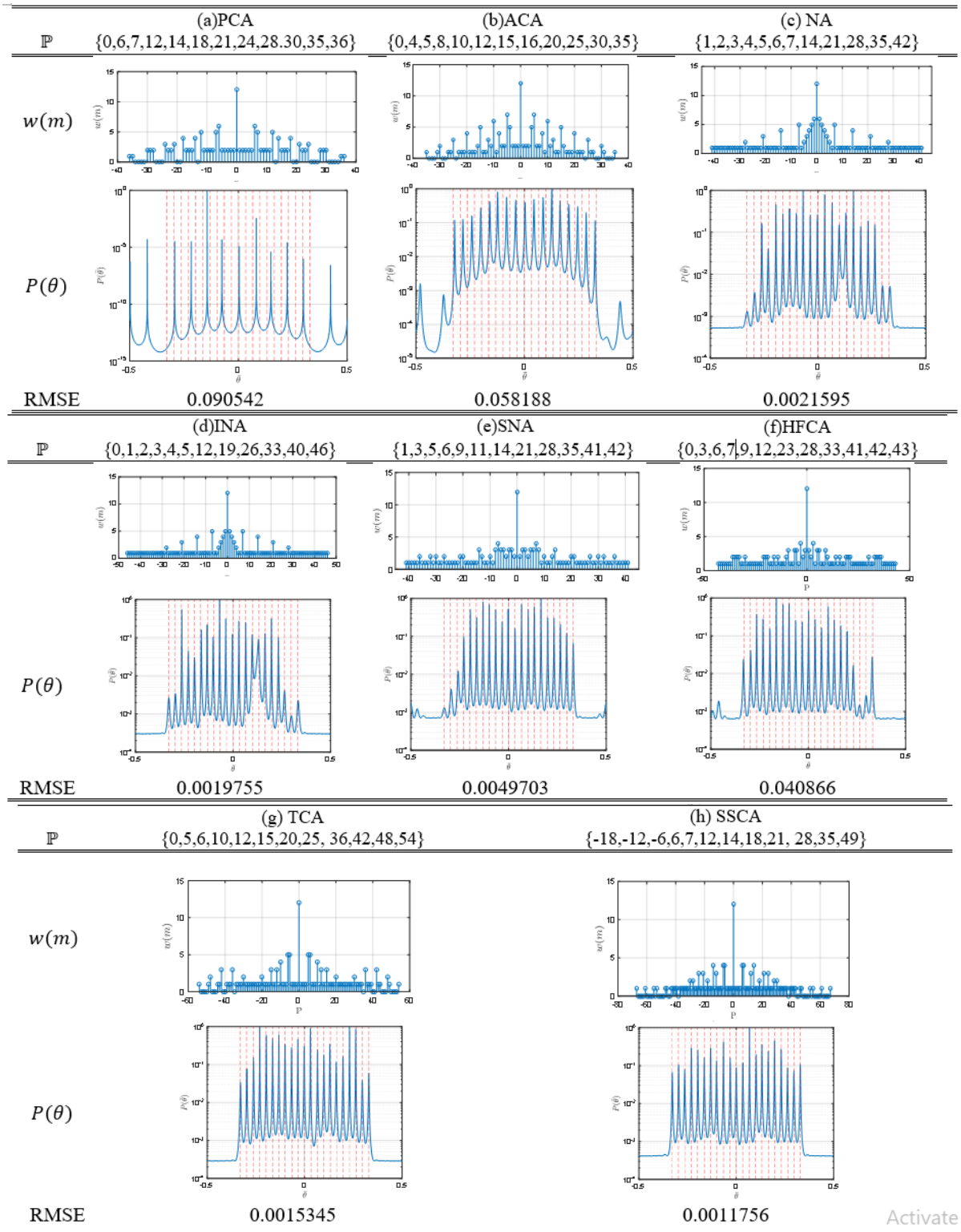

Figure 7. Comparison among (a) PCA, (b) ACA, (c) NA, (d) INA, (e) SNA,(f) HFCA, (g) TCA and (h) SSCA array configurations and the MUSIC spectrum $P(\theta)$

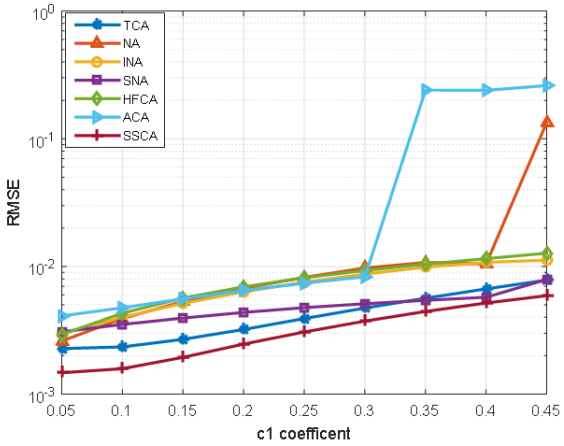

Figure 8. RMSE vs. c_1 coefficient

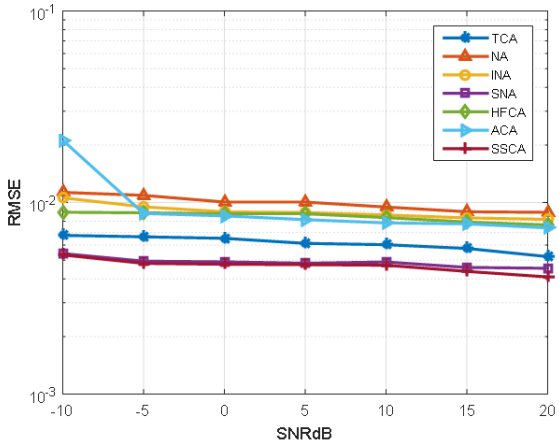

Figure 9. RMSE vs. SNR

weight function $(w(1), w(2), w(3))$ is $(1, 1, 1)$ as the TCA array, while the weight functions for PCA, ACA, NA, INA, SNA and HFCA are (2,2,2); (2,2,2); (6,5,4); (5,4,3); (2,3,3) and (3,2,4) respectively. Nested arrays have the highest weight functions since the dense array creates a triangular area at the center. From the observed weight function, the proposed SSCA array outperforms the other array structures since it has a smaller number of interfered virtual elements, a higher DOF, and an aperture size. The third row shows the MUSIC spectrum, it can be shown that the SSCA array can resolve all the sources effectively since it demonstrates the true peaks for all sources. The proposed SSCA array outperforms other array types that introduce spurious peaks and high error estimation.

Furthermore, the estimation accuracy is evaluated by the root mean square error (RMSE), which is expressed as:

$$RMSE = \sqrt{\frac{1}{M_c Q} \sum_{mc=1}^{M_c} \sum_{q=1}^{Q} (\bar{\theta}_{M_c,q} - \theta_q)^2} \qquad (32)$$

where $\bar{\theta}_q$ is the estimated DOA of the q-th source for m_c Monte Carlo trials, and θ_q is the actual DOA. The first scenario considers the variation of the coupling coefficient value ($| c |$) from 0,05 to 0.45. The simulation parameters in this scenario are set as follows, number of elements=10, =12 within the range $\bar{\theta} = [-0.3, 0.3]$, $SNR = 10$, $B = 100$, snapshots=1000, and the number of trials is 200. The result is shown in figure 8. It can be noticed that RMSE is progressively increasing with the increase of ($|c_1|$) for all the array types. The proposed SSCA has the lowest RMSE than other array types due to the less mutual coupling effect since the weight function of the first three lags is minimized to one and the more virtual elements in the DCA. Figure 9 shows RMSE curve with respect to SNR ranging from -10dB to 20dB, and other simulation parameters is set to number of elements=10, snapshots=1000, Q=12 within range $\theta[-0.3, 0.3]$, the number of trials is 200, and mutual coupling coefficient $c_1 = 0.3e^{(j\pi/3)}$. It can be noticed that the proposed SSCA and SNA have the lowest RMSE compared to other array types although the weight function of the first three lags of SNA w(1)=w(3)=1 and w(2)=4, but it has 29 uDOFs. NA has the worst performance due to the dense subarray that results in a hard mutual coupling effect. Figure 10 shows the RMSE curve with respect to the number of snapshots ranging from 200 to 2000, SNR =10dB, and the other simulation parameters as in the previous scenario. Again, it can be noticed that the proposed SSCA and SNA have the lowest RMSE compared to other array types for the same reason as mentioned previously. NA has the worst performance due to the dense subarray that results in a hard mutual coupling effect.

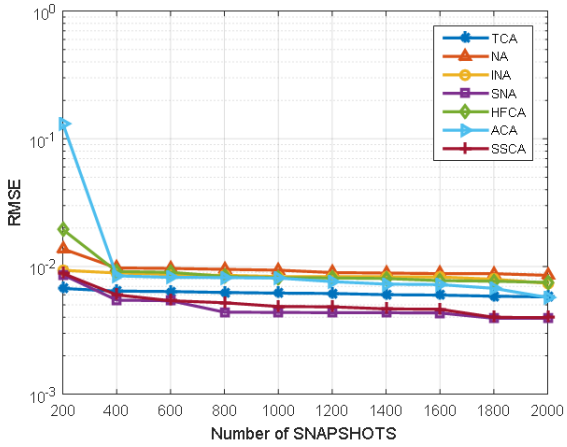

Figure 10. RMSE vs. number of snapshots

5. Conclusions

A new coprime array is proposed that studies the most important properties of recently developed non-uniform linear arrays. The proposed array point of view is to design a sparse array that has a large number of contiguous lags with small inter-element separations of element pairs. By

dividing one of the subarrays into two segments, located in the positive and negative axis sides, and moving the 0-lag position to a new position, a new coprime array is constructed with improved DOFs and less mutual coupling. The mathematical expression of the contiguous lags is derived with respect to the first hole position. The numerical analysis shows that the DOA estimation of the SSCM array outperforms its rivals using the same number of elements.

References

[1] J. Krim and M. Viberg, "Two decades of array signal processing research: the parametric approach," *IEEE Signal Process.*, vol. 13, pp. 67–94, 1996.

[2] H. Van Trees, "Optimum array processing: part iv of detection, estimation, and modulation theory," *Wiely*, 2002.

[3] F. A. Salman and B. M. Sabbar, "Doa estimation exploiting moving platform of unfolded coprime array," *International Journal of Intelligent engineering and systems*, vol. 15, pp. 532–542, 2022.

[4] E. BouDaher, F. Ahmad, M. Amin, and A. Hoofar, "Mutual coupling effect and compensation in non-uniform arrays for direction-of-arrival estimation," *Digit. Signal Process. A Rev. J.*, vol. 16, pp. 3–14, 2017.

[5] F. A. Salman and B. M. Sabbar, "Coprime array parameters optimization for doa estimation,," *Iraqi Journal of Information and Communications Technology(IJICT)*, vol. 4, pp. 23–39, 2021.

[6] R. Schmidt, "Multiple emitter location and signal parameter estimation," *IEEE Trans. Antennas Propag.*, vol. 34, pp. 276–280, 1986.

[7] T. Roy, R. Kailath, "Esprit-estimation of signal parameters via rotational invariance techniques,," *IEEE Transactions on Acoustics, Speech, and Signal Processing*, pp. 984–995, 1989.

[8] F. A. Salman and B. M. Sabbar, "Estimation of coherent signal on modified coprime array," *in: proc. 16th International Middle Eastern Simulation and Modelling Conference (MESM)*, 2020.

[9] Z. Zheng, Y. Wang, Y. Kong, and Y. Zhang, "Misc array: a new sparse array design achieving increased degrees of freedom and reduced mutual coupling effect," *IEEE Trans. Signal Process.*, vol. 67, no. 7, pp. 276–280, 2019.

[10] A. Moffet, "Minimum-redundancy linear arrays," *IEEE Trans. Antennas Propag.*, vol. 16, no. 2, pp. 172–175, 1968.

[11] G. S. Bloom and S. W. Golomb, "Applications of numbered undirected graphs," *Proc. IEEE*, vol. 65, no. 42, pp. 562–570, 1997.

[12] F. A. Salman and S. B. M., "Doa estimation exploiting moving platform of unfolded coprime array," *International Journal of Intelligent Engineering Systems*, vol. 15, no. 2, pp. 532—542, 2022.

[13] C. L. Liu and P. P. Vaidyanathan, "Maximally economic sparse arrays and cantor arrays," *in: ICAMSAP 2017, IEEE 7th Int. Work. Comput. Adv. Multi-Sensor Adapt. Process*, pp. 1–5, 2017.

[14] P. Pal and P. P. Vaidyanathan, "Nested arrays: A novel approach to array processing with enhanced degrees of freedom," *IEEE Trans. Signal Process.*, vol. 58, no. 8, pp. 4167—4181, 2010.

[15] P. P. Vaidyanathan and P. Pal, "Sparse sensing with co-prime samplers and arrays," *IEEE Trans. Signal Process.*, vol. 59, no. 2, pp. 573—-586, 2011.

[16] M. Yang, L. Sun, X. Yuan, and B. Chen, "Improved nested array with hole-free dca and more degrees of freedom," *Electron. Lett.*, vol. 52, no. 25, pp. 2068–207, 2016.

[17] C. L. Liu and P. P. Vaidyanathan, "Super nested arrays: linear sparse arrays with reduced mutual coupling - part i: Fundamentals," *IEEE Trans. Signal Process.*, vol. 64, no. 15, pp. 3997—4012, 2016.

[18] J. Liu, Y. Zhang, Y. Lu, S. Ren, and C. S, "Augmented nested arrays with enhanced dof and reduced mutual coupling," *IIEEE Trans. Signal Process.*, vol. 65, no. 21, pp. 5549—5563, 2017.

[19] J. Shi, G. Hu, H. Zhou, and X. Zhang, "Generalized nested array: optimization for degrees of freedom and mutual coupling," *IEEE Commun. Lett.*, vol. 22, no. 6, pp. 1208—1021, 2018.

[20] P. Pal and P. P. Vaidyanathan, "Coprime sampling and the music algorithm," *in: (DSP/SPE 2011) Digital Signal Processing and Signal Processing Education Meeting*, 2011.

[21] S. Qin, Y. D. Zhang, and M. G. Amin, "Generalized coprime array configurations for direction-of-arrival estimation," *IEEE Trans. Signal Process.*, vol. 63, no. 6, pp. 1337—1390, 2015.

[22] A. Raza, W. Liu, and Q. Shen, "Thinned coprime arrays for doa estimation," *in: (EUSIPCO 2017) 25th Eur. Signal Process. Conf.*, pp. 395—399, 2017.

[23] C. L. Liu and P. P. Vaidyanathan, "Remarks on the spatial smoothing step in coarray music," *IEEE Signal Process. Lett.*, vol. 22, no. 9, pp. 1438—1442, 2015.

[24] A. Raza, W. Liu, and Q. Shen, "Thinned coprime array for second-order difference co-array generation with reduced mutual coupling," *IEEE Trans. Signal Process.*, vol. 67, no. 8, pp. 2052—2065, 2019.

[25] X. Wang and X. Wang, "Hole identification and filling in k-times extended co-prime arrays for highly efficient doa estimation," *IEEE Trans. Signal Process.*, vol. 67, no. 10, pp. 2693—2706, 2019.

[26] P. Ma, J. Li, F. Xu, and X. Zhang, "Hole-free coprime array for doa estimation: augmented uniform co-array," *IEEE Signal Process. Lett.*, vol. 28, pp. 36—40, 2020.

[27] Y. Zhang, M. Yang, X. Zhang, S. Han, and J. Cao, "The limited aperture sparse array for doa estimation of coherent signals: A mutual-coupling-optimized array and coherent doa estimation algorithm," *Advances in Sparse Array Signal Processing and its Applications*, 2022.

[28] M. Ebrahimi, M. Karimi, and M. Modarres-Hashemi, "Optimal sparse linear array design with reduced mutual coupling effect," *AEU- International Journal of Electronics and Communications*, vol. 170, 2023.

[29] W. Y. B. B. B. M. F. Wang, Y.an Cui, "Symmetric thinned coprime array with reduced mutual coupling for mixed near-field and far-field sources localization," *IET Radar Sonar Navig*, vol. 16, p. 1292–1303, 2022.

[30] G. Zhang, Y.and Hu, F. Zhang, and H. Zhou, "Enhanced cacis configuration for direction of arrival estimation," *Electronics Letters*, vol. 58, no. 19, p. 737–739, 2023.

[31] S. Zhang, Z. Zhou, G. Cui, X. Tang, and P. Fan, "Enhanced low-redundancy restricted array for direction of arrival estimation," *arXiv:2208.05263*, 2023.

[32] A. M. A. Shaalan, J. Du, and Tu, "Tcla array: a new sparse array design with less mutual coupling," *in: ICASSP 2021, IEEE International Conference on Acoustics, Speech and Signal Processing*, 2021.

[33] F. A. Salman and B. M. Sabbar, "Low-complexity doa estimation method based on joined coprime array," *Journal of Telecommunications and Information Technology*, no. 1, pp. 11–16, 2024.

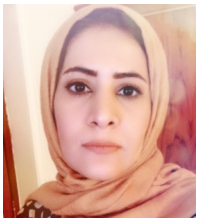

Fatimah A. Salman received her B.Sc. Degree in computer engineering from the University of Technology, M.Sc. Degree in Network Engineering and a Ph.D. in Information and Communication Engineering from Al-Nahrain University, Iraq. She works in College of Information Engineering, /Al-Nahrain University. Her fields of interest are Mobile Networks, Applications of Signal Processing in Direction Finding, beamforming, and Wireless Communication. .

Dr. Bayan Mahdi Sabbar received his B.Sc. in Electrical Engineering, in 1980, M.Sc. in Digital Communications Systems, in 1983, and Ph.D in (Electrical Engineering) in 1987. He works at Al-Mustaqbal University College, Baghdad, Iraq. His fields of Interest are Adaptive systems, high-resolution algorithms and their applications, Applications of Signal Processing in Direction Finding and Image Processing, and identification systems based on Signal Processing.